SUPPORTING INFORMATION

High Output Triboelectric Nanogenerator based on 2D Boron Nitride Nanosheets-PVP Composite Ink and Electrospun Cellulose Acetate Nanofibers for Kinetic Energy Harvesting and Self-Powered Tactile Sensing Applications

Ainikulangara Sundaran Bhavya[1,2], Hasna M. Abdul Hakkeem[1,2], Saju Pillai [1,2], Achu Chandran[1,2*], Kuzhichalil Peethambharan Surendran[1,2*]

[1]Materials Science and Technology Division, CSIR- National Institute for Interdisciplinary Science and Technology (CSIR-NIIST), Industrial Estate P.O., Thiruvananthapuram -695019, India

[2]Academy of Scientific and Innovative Research (AcSIR), Ghaziabad- 201002, India

[*] E-mail: kpsurendran@niist.res.in

[*] E-mail: achuchandran@niist.res.in

TEM images of pristine h-BN and exfoliated BNNSs:

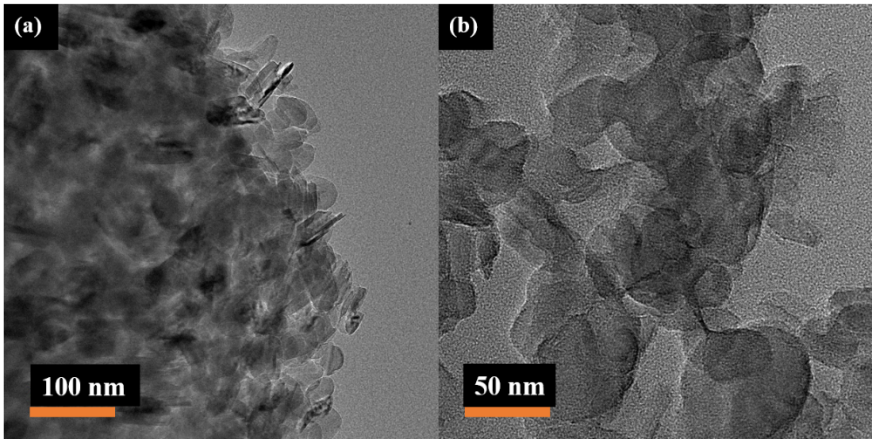

Figure S1: TEM images of (a) pristine h-BN and (b) BNNSs that were exfoliated from pristine h-BN.

It is possible to identify the morphological changes of bulk h-BN following liquid phase exfoliation by using TEM microscopic studies. Sample dispersions were utilised in the TEM analysis process. The TEM images represented in Figure S1(a) and (b) demonstrate the formation of BNNSs from its pristine h-BN material by the sonication-assisted liquid phase exfoliation method. The bulky parent h-BN counterpart in Figure S1(a) is considerably larger size and also has a morphology resembling a stacked sheet structure. BNNSs shown in Figure

S1(b) possess a translucent, ultrathin flat structure. It indicates that the h-BN sheets have been exfoliated into separate individual layers. The continuous solvent interaction with the material particles causes the separation of stacked layers into individual sheets of reduced lateral dimension by sonication-assisted exfoliation in a liquid media.

Structural analysis of bulk and exfoliated h-BN:

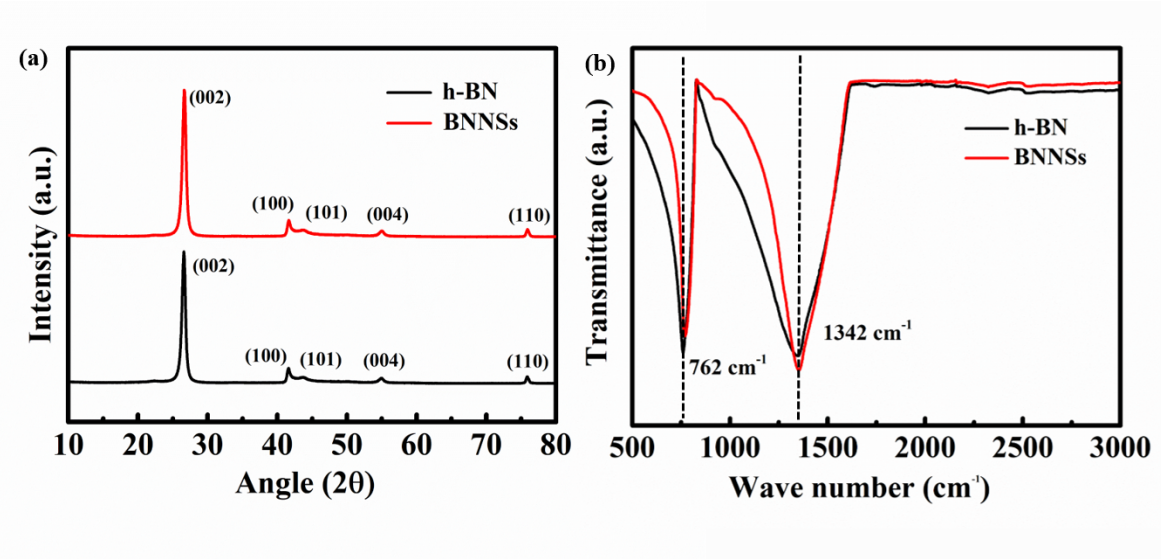

Figure S2: (a) XRD analysis (b) FTIR spectra of parent h-BN and exfoliated BNNSs.

X-ray powder diffraction (XRD) was used to further characterise the crystalline structure of both exfoliated and bulk h-BN. Figure S2(a) clearly shows the diffraction peaks observed at angles $2\theta = 26.6°$, 41.6°, 43.7°, 54.9°, and 75.9°, which indicates the (002), (100), (101), (004) and (110) crystallographic planes of h-BN respectively. The enhanced intensity of the XRD crystal plane (002) in the exfoliated sample confirms the effective exfoliation of bulk h-BN. The higher intensity value of the (002) plane in BNNSs indicates that the crystal plane is more exposed and that exfoliation occurs along this plane without causing any damage to the crystal structure.

Figure S2(b) represents the FT-IR analysis of h-BN and exfoliated BNNSs. The spectral region of 500–3000 cm^{-1} was analysed to determine the bonding type of h-BN. The in-plane stretching and the out-of-plane bending vibrations of h-BN are represented by the two distinct absorption peaks at 1342 cm^{-1} and 762 cm^{-1}, respectively. A minor blue shift was found from 1342 cm^{-1} and 762 cm^{-1} to 1355 cm^{-1} and 771 cm^{-1} after exfoliation. This blue shift that was seen can be explained by the thickness reduction in BNNSs when it exfoliated from its bulk precursor.

Thermal property analysis of PVP and BN-PVP composite ink

Thermogravimetric analysis (TGA) was used to analyse the thermal degradation behavior of pure PVP and dried BN-PVP composite ink, The thermogram curves of PVP and BN-PVP depicted in Figure S3 were obtained by heating the sample at a rate of 10°C/min under argon gas atmosphere. The TGA curve of pure PVP displays a single primary degradation step that is observed in a temperature window between 100°C and 550°C. The observed 90% weight loss of the polymer starts at 100°C and continues up to 550°C. The weight loss is comparably less in BN-PVP composite ink because of the presence of BNNSs as filler material, its higher thermal stability contributes to the weight loss reduction in the composite sample.

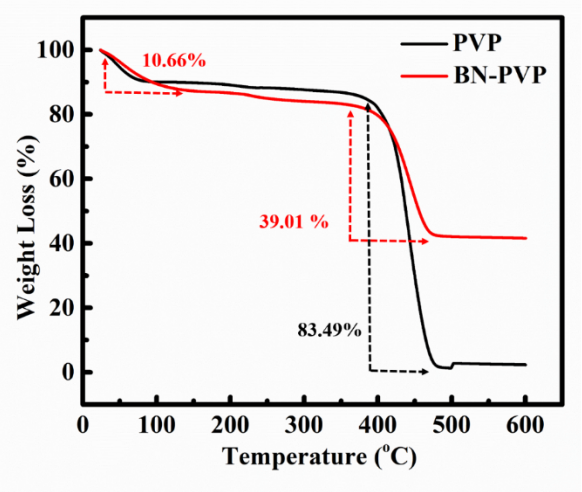

Figure S3: TGA analysis of PVP and BN-PVP ink.

Force sensitivity study of the tactile sensor at higher force levels

We have conducted the force sensitivity study of the tactile sensor at different higher force levels (20 N-150 N) shown in Figure S4(a) below. Even after 10 N force, the voltage curve shows an increasing trend. At higher force ranges the slope of the curve becomes lower value also the sensitivity decreases shown in Figure S4(b).

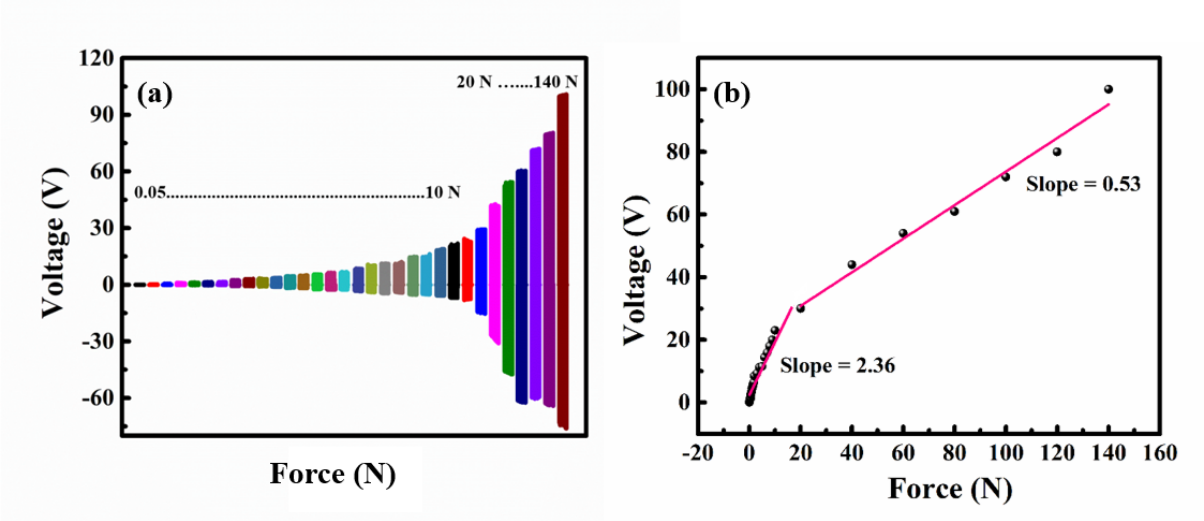

Figure S4: (a) Force sensitivity study in higher force ranges from 20 N to 150 N. (b) Sensitivity analysis in the higher force window.

Effect of BNNS concentration and TENG output

It is clear that BNNS content in screen-printed films influences the enhancement of BN-PVP/ES-CA TENG output, we have analyzed BN-PVP/ES-CA TENG's output voltage and current density with different weight percentages of BNNSs, which are shown in the Figures S5 (a & b)). The output voltage and current rise significantly with increasing BNNS concentration. The percentage of BNNSs contributes to the net output performance because the increasing concentration shifts the electron affinity of the composite structure stronger towards the more negative side of the triboelectric series. In combination with positive ES-CA material, more charge transfer takes place with a greater percentage of BNNSs.

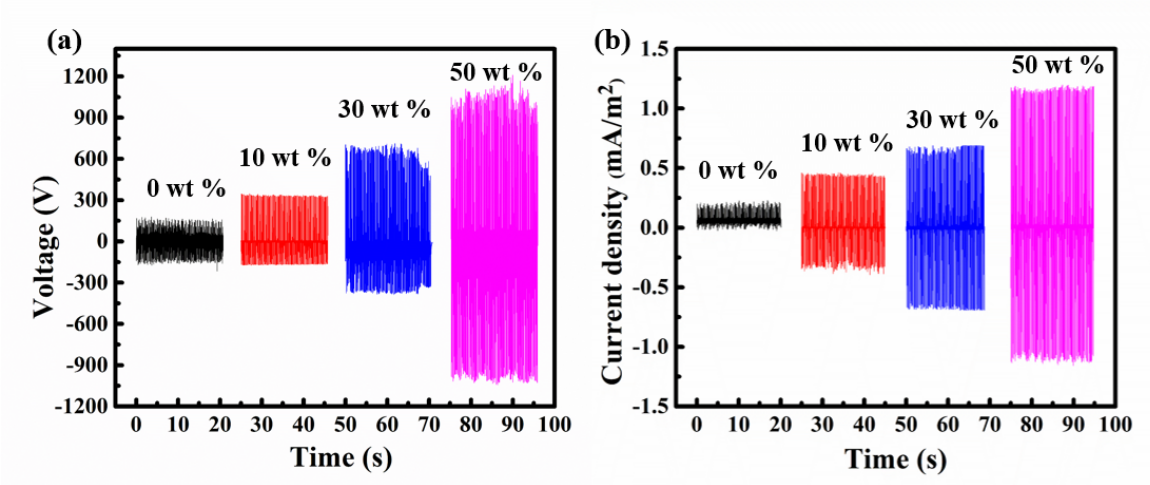

Figure S5: (a) Output voltage and (b) short-circuit current density of BN-PVP/ES-CA TENG with different weight percentages of BNNSs

Energy harvesting application of BN-PVP/ES-CA TENG

The photographic image of the BN-PVP/ES-CA TENG powering small-scale electronic devices like a digital thermometer and a calculator. Small-scale electronic devices can be powered by using this high-output TENG.

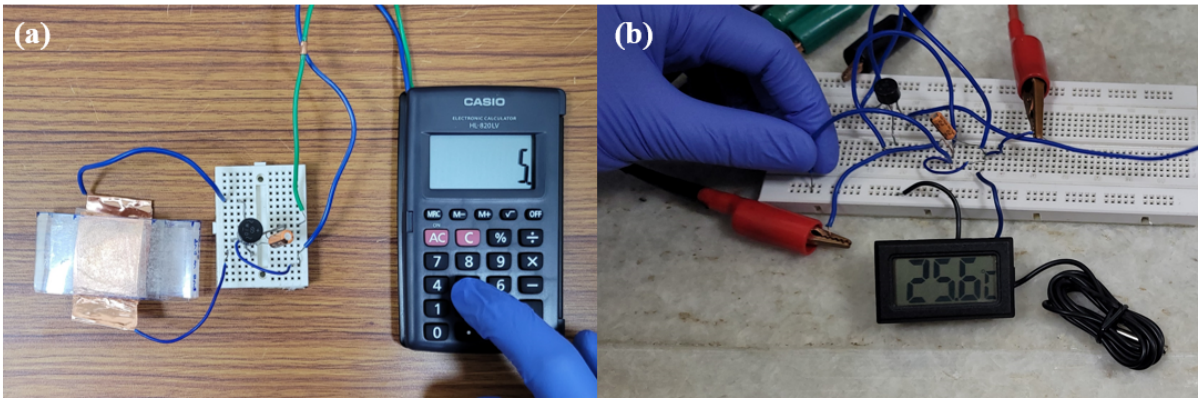

Figure S6: Powering electronic devices using BN-PVP/ES-CA TENG

Table summarising the performance of printed TENGs:

The output performance of various cellulose-based TENGs [1,7] is summarized in Table T1. The BN-PVP/ES-CA TENGs that are screen-printed have the potential to offer a power density that is significantly higher than the TENGs based on cellulose that have been documented.

Table T1: A summary of the output performance of different TENGs based on cellulose is provided. (Triboelectric materials used, substrate, electrode materials used, power density, and reference are included)

Sl No.	**Triboelectric materials used**	**Substrate**	**Electrode**	**Power density**	**Ref**
1	Bacterial nanocellulose	Flexible polypropylene (PP) film	Copper (Cu)	4.8 mW/m^2	[1]
2	Cellulose nanofiber (CNF)/phosphorene	Polyethylene terephthalate (PET)	Gold (Au)	1.06 µW/ cm^2	[2]
3	Cellulose nanofiber/ Silver (Ag) nanowire	……..	Ag nanowire	693 mW/m^2	[3]

4	Cellulose nanofiber/ PDMS	PET	Ag	29 mW/m^2	[4]
5	Cellulose-$BaTiO_3$ /PDMS	PTFE	Al	0.352 W/m^2	[5]
6	Cellulose aerogel /PTFE	Acrylic	Al	127 mW/m^2	[6]
7	Triethoxy-1H,1H,2H,2H-tridecafluoro-n-octylsilane (PFOTES) grafted cellulose nanofibrils/ polyamide	PMMA	Cu	1.35 μW/cm^2	[7]
8	**Boron nitride nanosheets (BNNSs) composite ink (BN-PVP) /Cellulose Nanofibers**	**BoPET**	**Cu**	**1.4 W/m^2**	**Present work**

We compared the relevant aspects of our research work with some available reference papers in the field of 2D material-based TENGs are also included in Table T2. Table T2 summarizes a comparison of the power densities in the proposed BN-PVP/ES-CA TENG with those of the TENGs that have been reported using other 2D materials in the literature[1,7]. Remarkably, screen-printed BN-PVP/ES-CA TENGs could deliver a power density that is better than the documented works in the domain of 2D material-based TENGs.

Table T2: A summary of the performance of various TENGs using 2D materials (Triboelectric materials used, durability, and reference are included)

Sl No.	Triboelectric materials used	Power output	Durability/ Flexibility	Ref
1	Graphene, PDMS, PET	0.14 W/m^2	…….	8
2	MoS_2 active layers synthesized onto the SiO_2/Si wafer, PDMS	.0225 W/m^2	Durable up to 10000 cycles /	9
3	Self-poled molybdenum disulfide embedded polyvinylidene fluoride (MoS_2@PVDF) hybrid nanocomposite, PET	.0654 W/m^2	Durable up to 10000 cycles	10
4	MXene/Glass, PET-ITO	0.52 W/m^2	Stable and reliable TENG output	11
5	MXene/PET-ITO	0.4 W/m^2	Stable and reliable TENG output	12
6	Au decorated WS_2, PTFE	.002 W/m^2	Durable upto 6000 cycles	13
7	Sandwich-structured polyimide (PI)/boron nitride nanosheet (BNNS)/PI nanocomposite	0.214 W/m^2	TENG showed good stability and flexibility	14
8	**Boron nitride nanosheets (BNNSs) composite ink (BN-PVP) /Cellulose Nanofibers**	**1.4 W/m^2**	**10000 cycles of durability and flexibility**	**Present work**

Reference:

(1) H. Kim, E. Yim, J. Kim, S. Kim, and J. Park, *Nano Energy*, 2017, **33**, 130–137.

(2) P. Cui, K. Parida, M. Lin, J. Xiong, G. Cai, and P. S. Lee, *Adv. Mater. Interfaces,* 2017, **1**(7), 1700651.

(3) I. Kim, H. Jeon, and D. Kim, *Nano Energy*, 2018, **53**, 975-981.

(4) C. Qian, L. Li, M. Gao, H. Yang, Z. Cai, B. Chen, Z. Xiang, Z. Zhang, and Y. Song,

Nano Energy, 2019, **63**, 103885.

(5) K. Shi, H. Zou, B. Sun, P. Jiang, J. He, and X. Huang, *Adv. Funct. Mater.,* 2020, **1**(9), 1904536.

(6) L. Zhang, Y. Liao, Y. Wang, S. Zhang, W. Yang, X. Pan, and Z. L. Wang, *Adv. Funct. Mater.,* 2020, **1**(9), *2001763*.

(7) S. Nie, Q. Fu, X. Lin, C. Zhang, Y. Lu, and S. Wang, *Chem. Eng. J.,* 2021, **404**, 126512.

(8) H. Chu, H. Jang, Y. Lee, Y. Chae, and J. H. Ahn, *Nano Energy,* 2016, **27**, 298-305.

(9) S. Park, J. Park, Y. Kim, S. Bae, T. Kim, K. Park, B. Hong, C. Jeong, and S. K. Lee, *Nano Energy,* 2020, **78**, 105266.

(10) B. Hedau, B. Kang, and T. J. Ha, *ACS Nano***,** 2022, **16**, 18355−18365

(11) Y. Dong, S. Mallineni, K. Maleski, H. Behlow, V. Mochalin, A. Rao, Y. Gogotsi, and R. Podila, *Nano Energy,* 2018**, 44**, 103-110.

(12) Y. Dong, S. Mallineni, K. Maleski, H. Behlow, V. Mochalin, A. Rao, Y. Gogotsi, and R. Podila, *Nano Energy,* 2018**, 44**, 103-110.

(13) T. Chekke, R. Narzary, S. Ngadong, B. Satpati, S. Bayan, and U. Das, *Sens. Actuators A: Phys.,* 2023, **349**, 114076.

(14) L. Pang, Z. Li, Y. Zhao, X. Zhang, W. Du, L. Chen, A. Yu, and J. Zhai, *ACS Appl. Electron. Mater.,* 2022, **4**, 3027-3035.